Nondestructive Testing and Evaluation

ISSN: 1058-9759 (Print) 1477-2671 (Online) Journal homepage: www.tandfonline.com/journals/gnte20

Failure patterns of solder joints identified through lifetime vibration tests

Kangkana Baishya, David M. Harvey, Teresa Partida Manzanera, Guangming Zhang & Derek R. Braden

To cite this article: Kangkana Baishya, David M. Harvey, Teresa Partida Manzanera, Guangming Zhang & Derek R. Braden (2023) Failure patterns of solder joints identified through lifetime vibration tests, Nondestructive Testing and Evaluation, 38:1, 147-171, DOI: 10.1080/10589759.2022.2084616

To link to this article: https://doi.org/10.1080/10589759.2022.2084616

Published online: 13 Jun 2022.

NONDESTRUCTIVE TESTING AND EVALUATION
2023, VOL. 38, NO. 1, 147–171
https://doi.org/10.1080/10589759.2022.2084616

Taylor & Francis
Taylor & Francis Group

Failure patterns of solder joints identified through lifetime vibration tests

Kangkana Baishya[a], David M. Harvey[a], Teresa Partida Manzanera[a], Guangming Zhang[a] and Derek R. Braden[b]

[a]General Engineering Research Institute, Faculty of Engineering and Technology, Liverpool John Moores University, Liverpool, UK; [b]Aptiv Services UK Limited, Binley Court, Coventry, UK

ABSTRACT

A method for non-destructively tracking the integrity of flip chip solder joints through life is investigated in this paper. An industry standard double-sided PCB was designed and manufactured with 14 flip chips to assess the failure patterns of each flip chip and each solder joint in lifetime vibration tests. Two configurations of PCB finish were tested, Electro Nickel Immersion Gold (ENIG) and Hot Air Surface Levelled lead (Pb HASL) using automotive industry manufacturing processes and quality standards. A random vibration test over a frequency range 10 Hz to 1000 Hz was specified by automotive engineers to replicate vibrations typically found on road vehicles. This vibration profile was applied to test circuit board assemblies (CBA) for 4-minute intervals until failure of all chips. At each interval test boards were extensively scanned by an acoustic micro-imaging (AMI) microscope to non-destructively measure parameters of solder joints. This enabled tracking of mechanical joint connection through-life. Methods were developed to process the large number of acoustic images of each solder joint and form metrics to evaluate solder joint integrity. Results from AMI show that the solder joints exhibit three distinct zones as they age: crack initiation, crack propagation and then failure.

ARTICLE HISTORY
Received 26 June 2021
Accepted 23 May 2022

KEYWORDS
Automotive electronics, random vibration test; mechanical failure, lifetime; nondestructive ultrasound imaging; reliability; solder joints

1. Introduction

In automotive, aerospace and military applications, electronic systems experience various dynamic loads and vibration frequencies under their operation [1–4]. Solder joint interconnects serve as electrical connections and mechanical supports, and the failure of a solder joint can cause electronic devices to malfunction [5]. Non-destructive testing of solder joints has never been more important in the wake of major incidents such as air crashes [6]. Evidence of cracking of solder and circuit disconnection on in-flight electronic control circuits was detected after the Air Asia crash of 2014. Factors such as operational cycles including thermal and vibration cycling during flight must be evaluated to ensure safe operation over extended periods. Any failure can be catastrophic and lead to loss of life. A survey by the US Air force reveals that about 55% of the failures of electronic equipment are due to high temperature and thermal cycling, 20% are related to

CONTACT David M. Harvey d.m.harvey@ljmu.ac.uk

vibration and shock, and another 20% are due to humidity [7]. In terms of product reliability, solder interconnects or joints can be the weakest link [8]. Since thermal cycling appears to be the major cause of electronic component failure, most of the previous work has investigated thermal loading and its cause on the failure mechanisms of solder joints. However, work considering random vibration loading for harsh applications is limited [9–13]. The aim of this work is to investigate the effects of vibration on the reliability of area array solder joints found on semiconductors used in automotive electronics. The vibration profile applied was developed by Aptiv dynamics experts based on multiple customer and international testing standards. The resultant profile was decelerated to produce a typical on-road random vibration profile, representative of non-engine mounted electronic products. The work is also unusual in that testing was carried out at room temperature without any thermal excitation [14] to isolate thermal effects and gain a better understanding of vibration effects.

Solder joint reliability vibration testing is expected for all electronics likely to experience harsh high cyclic fatigue environments such as vibration [15]. Consequently, designs must be made more resilient where possible. This usually involves ensuring resonances and their natural harmonics found in the mechanical design of a product are moved outside the vehicle vibration profile. However, none of the studies conducted so far have successfully conducted real time vibration lifetime tests or were able to monitor the exact dynamics of solder joint reliability. Solder joint reliability of area array packaged parts are greatly affected by the floor plan of the Circuit Board Assembly (CBA), influenced by the surrounding components and thickness of the Printed Circuit Board (PCB) [16], and have never been extensively studied in a vibration environment. This paper investigates for the first time the reliability of solder joints in area array packages through real time vibration using a non-destructive solder joint health monitoring technique, extending previous work on through-life thermal cycling fatigue [17] by the application of a real time vibration profile, and non-destructively detecting changes of the mechanical integrity in the solder joints until their complete mechanical failure.

2. Background to the inspection methods

A method for non-destructive examination of solder joint degradation as they progress through their operational life comprising of exposure to vibration. Moreover, since all flip chip solder joints are hidden under the flip chip, an imaging system that can penetrate the die is required to successfully ‘see’ the joints. An advanced acoustic imaging system was used, having the capability to image through the top of the chip with sufficient accuracy to collect degradation information at each solder connection. The ultrasound imaging selected was based on a gated 2D C-scan. These Acoustic Micro Imaging (AMI) C-scans [18] are relatively fast but for a doubled-sided populated PCB scanning all the individual flip chips can still take several hours. The measurements to test solder joint integrity were based on the reflection of the ultrasound from the solder joint to flip chip mechanical connection as this is where cracks usually develop. Two metrics were used to track the degradation of joints, the reflected ultrasound intensity, and the reflected ultrasound area, as they both show measurable growth through-life.

Using experience gained from previous Accelerated Thermal Cycling (ATC) tests [16], the manufactured samples were vibrated for a chosen cycle time of 4 minutes. The sample interval was chosen to best track the degradation of solder joints through-life in order to efficiently measure the decrease in joint integrity. Each flip chip was ultrasonically imaged to monitor all the solder joints at that specific time interval. After imaging each flip chip, the samples were returned to the vibration machine for another cycle, and this process repeated until all flip chips had failed.

Reliability life testing is founded on using time compression techniques which expose the test subject to an increased exposure level of stress than experienced during its normal life. This results in precipitation of failures in the solder joints earlier than would be seen in a field environment. However, even these accelerated tests take a long time, so early indication of failure and lifetimes indicated during these tests can be incorporated into future prognostics to reduced test times, saving resources and giving earlier indication of predicted lifetimes to manufacturers. AMI is a method that can help track solder joint connections non-destructively through lifetime tests.

3. Materials and methods

3.1. Electronic circuit design and manufacture

Figure 1 shows the top and bottom view of the printed circuit board (PCB) with various area array packages custom designed at Delphi, Liverpool. The PCB is double layer FR4 laminate of 0.8 mm thickness. The board was available in two surface finishes: Electro Nickel Immersion Gold (ENIG) and Hot Air Surface Levelled lead (Pb HASL) to examine the impact of surface finish choice on solder interconnect reliability. The top side of each PCB has 8 flip chips while the bottom side has 6, making a total of 14 flip chips all of which are numbered as shown in Figure 1. Each flip chip has an area of 8898 × 3948 μm and thickness 725 μm, and under bump metallization (UBM) structure consisting of an Al/Ni/Cu stack with 102 μm pad size. Flip chips were mounted without any underfill

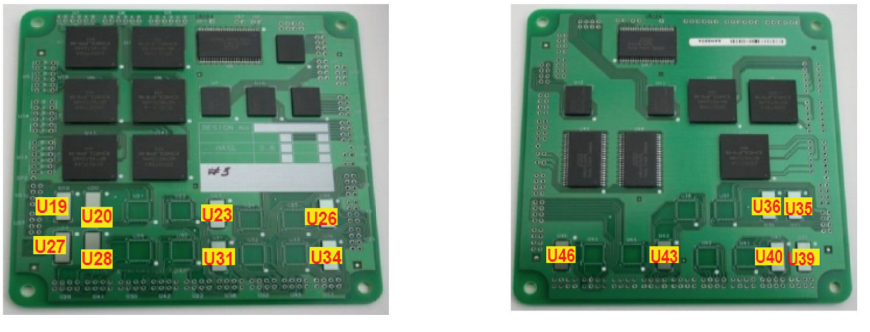

(a) Top Side of the PCB with the labelled flip chips under test

(b) Bottom Side of the PCB with the labelled flip chips under test

Figure 1. Test circuit board assembly layout with flip chip reference numbers [19]. Two images showing flip chip placement on printed circuit board with individual reference numbers. Figure 1(a) shows top side reflow, Figure 1(b) bottom side reflow.

onto the PCB using 109 solder joints spaced around the perimeter of the chips in two main rows. Whilst it is not normal practice to mount flip chips direct to PCB without underfill, in this instance the underfill was left out to reduce the test time. As a result, the solder joints will fail more quickly. However, it is suggested that they have the failure signature as if they were underfilled.

The solder composition was Sn = 52.9%, Pb = 45.9%, Cu = 1.2%, with solder bump diameter of 140 μm and solder bump height of 125 μm. The boards were soldered on a proprietary industry production line in Aptiv. All the flip chips are placed in different positions in the PCB and have different orientations relative to each other on opposite sides of the PCB as shown in Figure 2. Flip chips U23 and U26 are stand-alone flip chips with no back-to-back connections. U19-U35 and U20-U36 pairs are placed back-to-back with an offset along the breath (Figure 2(a)). U27-U39, U28-U40 pairs are placed back-to-back with an offset along the length (Figure 2(b)). U34-U46, U31-U43 pairs are placed back-to-back with no offset (Figure 2(c)). These different orientations were used to assess the effects of back-to-back placement offset on reliability, as well as each flip chip's position within the floorplan of a PCB [19]. Furthermore, the selection of die shape, rectangular as opposed to the more frequently used square die allows the study and influence of die shape on the failure distribution of solder joints on a package. The further a joint is from the neutral axes of the die or package, consequently corner joints are frequently reported in the literature as failing first.

An aluminium test adaptor plate, accommodating four test boards in a 4-5 mm recess supporting the edge of the board and secured in each corner using M3 Pan head screws to a torque of 1 Nm [19] and was designed and manufactured by Aptiv (formerly Delphi) (Figure 3). This adapter plate connects the shaker table to the test samples. It was designed and tested through simulation and measurement so that it contained no resonance frequencies inside the test frequency profile used. This ensures no influence on the test boards, other than applying the required excitation frequency and energy

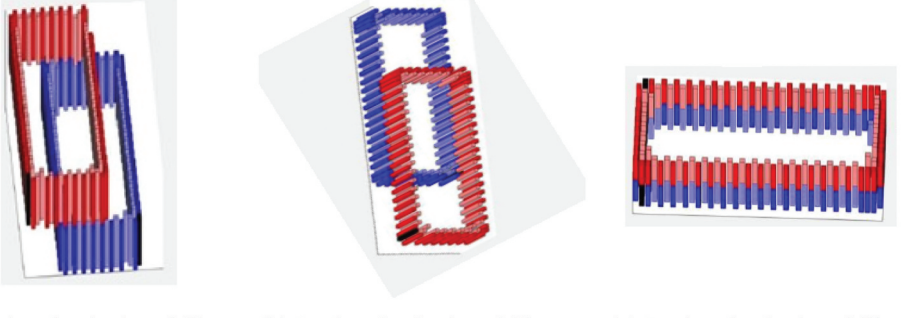

(a) Back to back placed flip chip orientation with offset along the breadth.

(b) Back to back placed flip chip orientation with offset along the length.

(c) Back to back placed flip chip orientation with no offset (mirrored).

Figure 2. Flip chip top (red) and bottom (blue) reflow side configurations to study individual bump behavioural response to applied test environment [20]. Three separate images illustrating rectangular flip chip orientation when placed over top of one another with printed circuit board between. Figure 2(a)offset along shortest edge. Figure 2(b) offset along longest edge. Figure 2(c) no offset, mirrored placement.

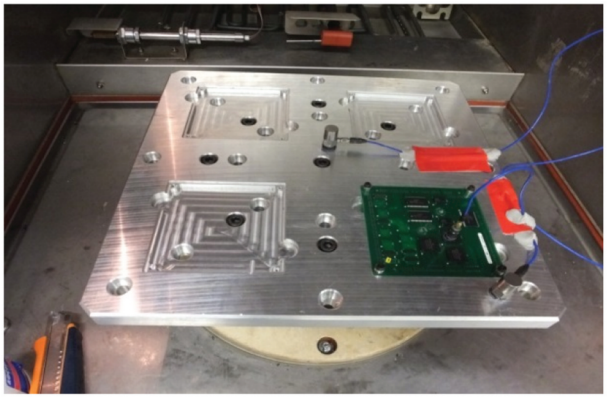

Figure 3. CBA mounted to aluminium test fixture mounted on the vibration table [19].

Table 1. Parameters of the random vibration profile used for this experiment: $G_{rms} = 9.47$ g.

Frequency (Hz)	10	20	50	100	200	300	400	500	750	1000
PSD $((m/s^2)^2/Hz)$	32	64	64	64	2	2	2	2	2	2

defined in the test profile. The random vibration profile used for the experiment was as Table 1. This profile, obtained with the help of automotive dynamics testing experts in Aptiv (formerly Delphi), is a low aggression accelerated representation of the vibration loading experienced by many automobiles in real life with a $G_{rms} = 9.47$ g [20].

3.2. Experimental setup

The circuit board assembly (CBA) was secured in the fixture mounted on the shaker and vibrated according to the random profile devised by Aptiv (formerly Delphi), Krakow. A practical resonance test was first conducted on an unpopulated PCB that showed the resonance point of the board to be around 212 Hz. This value was verified mathematically using Steinberg's equation for natural resonant frequency of a PCB fixed at four points as 219 Hz [7,19]. Good correlation is demonstrated between test and simulation, and consequently is lying in the lower energy region of the PSD documented in Table 1 resulting in minimal impact of fatigue life of the solder joints. As the total time to failure of all the flip chips in the CBA was unknown, a pre-test was conducted on both the ENIG and Pb HASL surface finish boards to determine their impact on solder joint lifetimes. For the ENIG surface finish boards, the flip chips were found to reach complete failure after 86 vibration cycles where each cycle is 4 minutes, equivalent to 5.73 hours or 20,640 seconds. For the Pb HASL surface finish boards, the flip chips were found to reach complete failure after 380 vibration cycles where each cycle is 4 minutes, equivalent to 25.33 hours or 91,200 [19]. The ultrasound C-scan images used in the solder joint through-life monitoring were obtained using the Sonoscan Gen6™ C-Mode Scanning Acoustic Microscope machine in the LJMU laboratory as shown in Figure 4. For through-life assessment the Gen6 was used for 2D Acoustic Micro Imaging (AMI) often called C-SAM. The labelling scheme of the

Figure 4. Sonoscan Gen6™ C-mode acoustic microscopy system (Image courtesy of Nordson/Sonoscan Inc).

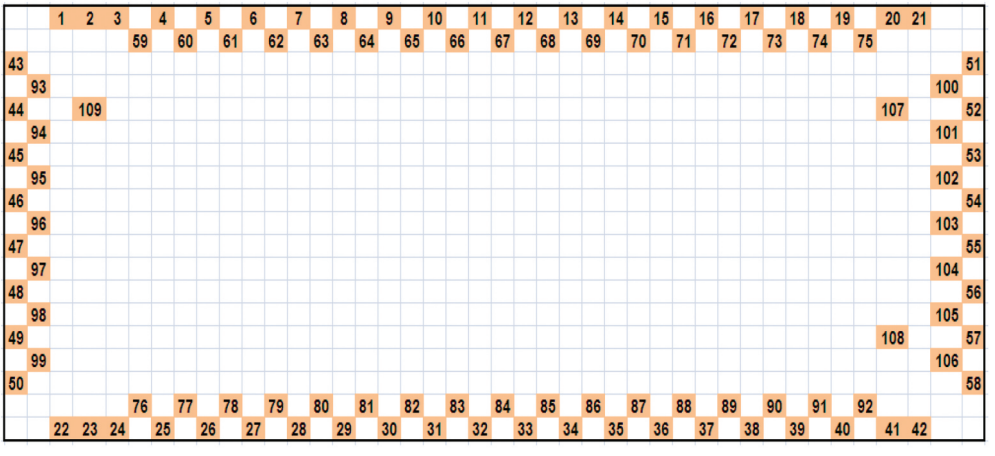

Figure 5. Labelling scheme for flip chip solder joints used in this study [21].

109 solder joints for analysis purposes along with a C-Scan of the solder joints in a flip chip are shown in Figures 5 and 6 respectively. A resolution of 3 micron was found to be optimal for scanning and recording solder joints after initial tests [19].

Based on the pre-test data, nine flip chips were selected according to their positions and relative orientations in the PCB for acoustic scanning at different scan intervals as shown in Table 2. The AMI scan intervals were chosen to gain at least eight data points when monitoring the lifetime from manufacture to failure. The acoustic images were then post processed as discussed in Section 4 using MATLAB.

The ultrasound imaging is non-destructive so enables lifetime monitoring of the degradation of all solder joints on flip chips by imaging through the silicon chip itself. As all 109 joints are hidden underneath each flip chip conventional optical imaging

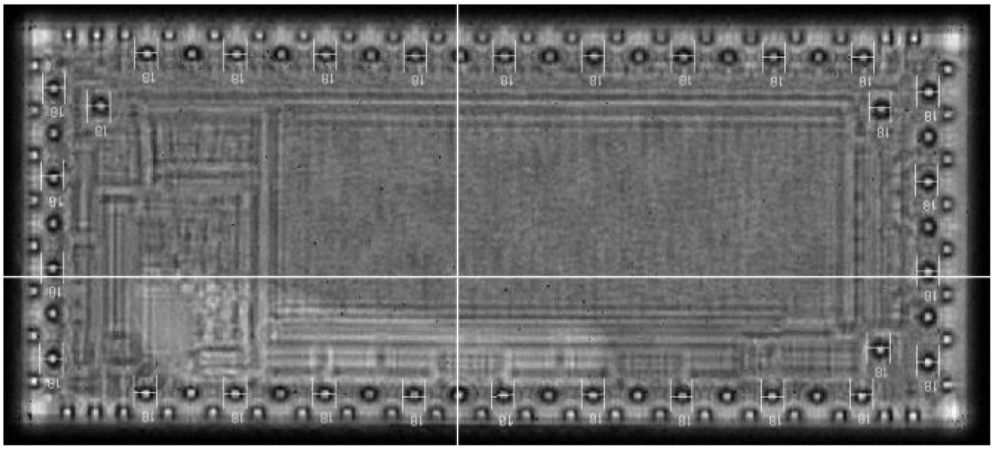

Figure 6. 230 mhz ultrasonic C-scan of a flip chip at 3 micron scan resolution showing 106 solder joints and some joint pixel measurements [19].

Table 2. Scan intervals for different flip chips for ENIG and Pb HASL CBA's.

ENIG	Scan interval 1 scan interval = 4 minutes	Pb HASL	Scan interval
U23	1 scan/cycle	U23	1 scan/cycle
U26	1 scan/2 cycles	U26	1 scan/2 cycles
U27	1 scan/5 cycles	U27	1 scan/5 cycles
U34	1 scan/5 cycles	U34	1 scan/5 cycles
U19	1 scan/5 cycles	U19	1 scan/10 cycles
U28	1 scan/10 cycles	U28	1 scan/10 cycles
U20	1 scan/10 cycles	U20	1 scan/10 cycles
U35	1 scan/5 cycles	U35	1 scan/20 cycles
U40	1 scan/5 cycles	U40	1 scan/20 cycles

cannot see all the joints and can only partially image the outer joints. However, after complete chip failure the chip detaches from the PCB and can be inspected under an optical microscope as shown in Figure 7.

4. Degradation analysis of the solder joints

Through-life degradation analysis was completed during the tests by removing the CBAs from the vibration chamber at the selected intervals to examine the solder joints using ultrasound/AMI. Once the first chip had failed, the remaining chips were scanned, and vibration testing was repeated using the same cycle times until all 14 flip chips had failed. In this work, we present the through-life analysis for CBA's with ENIG surface finish as a timelier experiment could be completed compared to Pb HASL surface finish within the confines of a three-year study. The acoustic images obtained via through-life monitoring were subjected to various stages of image processing using MATLAB, each of which will be discussed hereafter.

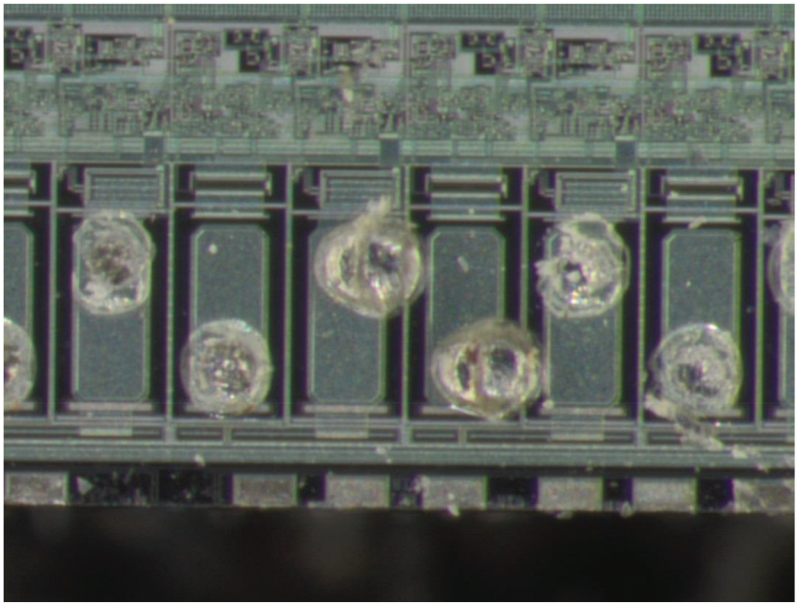

Figure 7. Magnified optical image of complete solder joint failure, residue from solder ball found on connection pad of the die.

4.1. Image intensity equalisation

As a result of the long duration (>12 months) of the experimental work, repeatability and measurement stability issues such as intensity and gain were found in the images due to the AMI system. Image equalisation was performed during post processing to compensate and overcome this and any further image acquisition variance. Consequently, images at time zero or zero cycles, for each flip chip were taken as a reference and used to calculate the mean intensities of all the other subsequent images. A scaling between each image with the reference image was determined using the formula:

$$\text{Scalingfactor(n)} = \text{mean\_of\_reference}/\text{mean\_of\_each image(n)}.$$

All the images were then multiplied with their corresponding individualised scaling to obtain the equalised images. Figure 8 shows the comparison of the acquired images with and without equalisation.

In order to ensure that the intensity equalisation does not affect the final results, the maximum intensity plots for a few of the solder joints of the flip chips were analysed. Figure 9 shows a comparison of the effect of equalisation on the maximum intensity of a solder joint 67 of flip chip U34. As can be seen from Figure 9, as the number of vibration cycles increases, mean intensity equalisation has minimal effect on the propagation pattern of the maximum intensity values. Since it does not affect the shape or propagation pattern, it will not have any significant effect on the results drawn from the data analysis. However, for lifetime analysis purposes only the mean intensity and area of the solder joints were used as metrics. This is because mean intensity and area are more reliable measures compared to maximum intensity whose values can be directly affected by any mismatches in the gain of the AMI system.

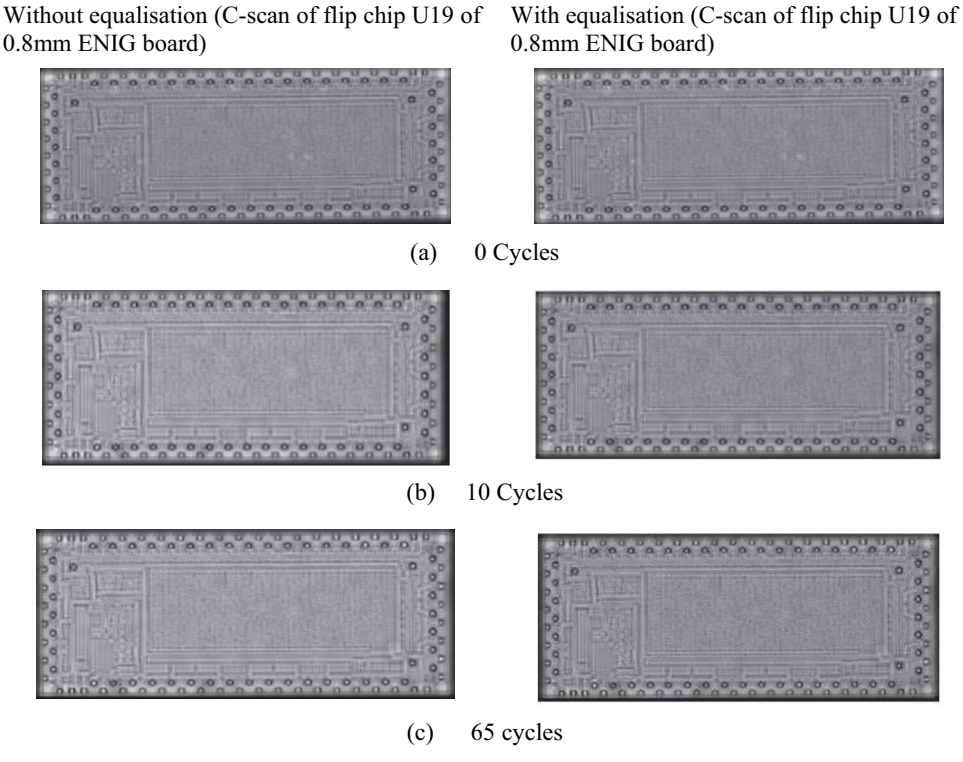

Figure 8. Comparison of images with and without equalisation for flip chip U19 at various scan cycles.

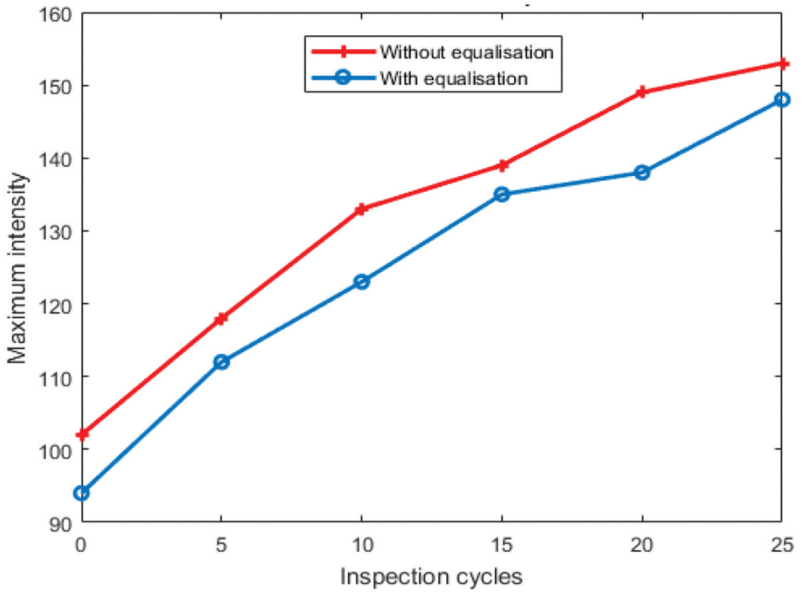

Figure 9. Comparison of the maximum intensity of the solder joint 67 of U34 with and without equalisation.

4.2. Joint selection and thresholding

Once the intensity/gain mismatches were corrected as illustrated in section 5.1, MATLAB coding was used to select individual solder joints for degradation analysis. Then, the first step to carry out the analysis was thresholding. Thresholding is a simple but effective technique of image segmentation. For most images, in general, the grey levels of pixels belonging to an object are substantially different from the grey level of the background. An appropriate threshold value can be set to differentiate the object and the background. For example, any pixels with values either greater than or less than a threshold value are treated as the main object and the rest are considered as background. The most important parameter in a thresholding technique is the decision of the threshold value. Many features in the image can be used to set the threshold parameter, for example, histogram [22,23], and gradient information [24].

Yang [17] observed in his work on thermal cycling effects on solder joints, that as the solder joints degraded their intensity increased considerably for fractured joints while there was not much change when it came to healthy joints. Therefore, to verify if this is the case with vibration cycling, and also to get a rough overview of how the flip chip intensities change with an increase in the number of vibration cycles, the greyscale AMI images are converted to binary images using Otsu's thresholding [25]. The binary images are then masked over the original image to get a threshold image. Figure 10 shows the implementation of Otsu's method and subsequent masking of the original image with an Otsu masked image. As can be observed from the image, Otsu's thresholding method provides a distinct region of interest for further image analysis.

On implementing Otsu's thresholding method to the acoustic images of the solder joint 67 of flip chip U19 obtained throughout vibration cycling, it can be seen from Figure 11 that as the vibration cycling progresses, the intensity and area around the centre of the solder joint increases. The same pattern was generally observed with all 109 solder joints in all the flip chips across all the scans (about 100) that were selected for through-life monitoring using AMI. Moreover, this observation confirms that as in thermal cycling [17], for vibration cycling the intensity and area of the solder joints also increase with vibration cycles. Hence, these parameters can be used to analyse the

Figure 10. Implementation of Otsu's method and masking. Three separate images of solder joints illustrating the implementation of Otsu's thresholding method used to convert greyscale AMI images to binary images. Figure 10(a) shows the original AMI image of a solder joint. Figure 10(b) shows the Otsu masked image of Figure 10(a). Figure 10(c)shows the Otsu masking of Figure 10(a)using the Otsu masked image from Figure 10(b). The Figure shows that Otsu's thresholding method provides a distinct region of interest for image analysis.

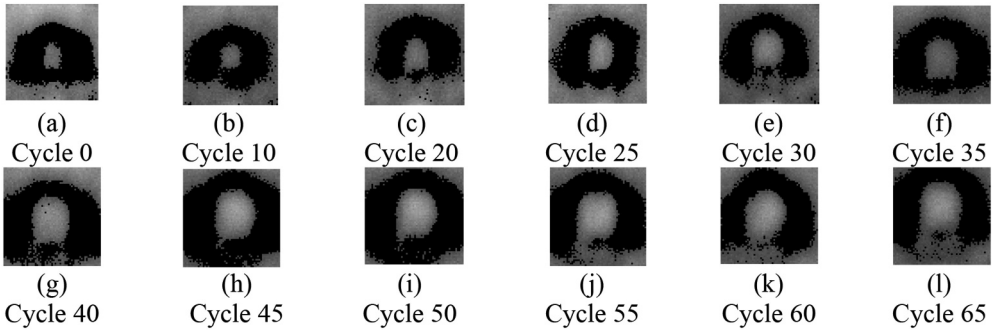

Figure 11. Implementation of Otsu threshold and mask on joint 67 of flip chip U19 acquired AMI images at accumulated vibration test cycles. Twelve separate images of the Otsu thresholding method used to convert AMI images of solder joint 67 of flip chip U34 throughout vibration cycling. Figure 11 (a–l)sequentially show evolution of Otsu threshold and mask image of the solder joint from 0 to 65 vibration cycles.

degradation patterns of the solder joints. Typically, the focused ultrasonic spot size resolution at 230 MHz is 10–15 microns, but the transducer used can actually detect defects smaller than its resolution by an order of magnitude [18]. This gives a benefit that even if defects may not be precisely resolved they can be detected, and the detected features tracked in a way which may be used to indicate degradation to failure throughout joint life. Features such as cracks in solder joints were examined previously in many cases destructively by cross-sectioning [3] and found to correspond with the ultrasound images taken as the joints degrade [17]. Furthermore, it was observed that solder joints for flip chips used in this study tend to crack along a catenary/parabolic line in the intermetallic boundary layer formed between the lead solder ball and Under Bump Metallisation (UBM) connection pad of the flip chip [21]. This subsequently informed the gating choice for the ultrasound scans to encompass this region.

4.3. Selecting the region of interest using masking

Since this region of interest (ROI) is a grey region inside the black ring obtained after thresholding, the next stage was to isolate this region for further processing. As presented in section 5.2, the joints to be analysed were individually selected using MATLAB coding. It was found that a rectangular area of 60×60 pixels is enough to isolate one solder joint. An adjustable elliptical mask was then used to separate out the region of interest as shown in Figure 12. As the region of interest is almost never a circular region, using an adjustable elliptical mask helps in isolating a much more accurate region of interest as illustrated in Figure 12. The grey region inside the black background now obtained is the region of interest (Figure 12(d)) used for subsequent analysis.

In AMI, the strength of the reflected echoes provides information about the selected solder joint interface. In this case, the solder joint to flip chip connection. As a solder joint fatigues and cracks, the acoustic reflections from growing air gaps provides an increase in intensity and reflected area. Therefore, both mean pixel intensities and area of the ROI are used to help determine the degradation patterns of all solder joints.

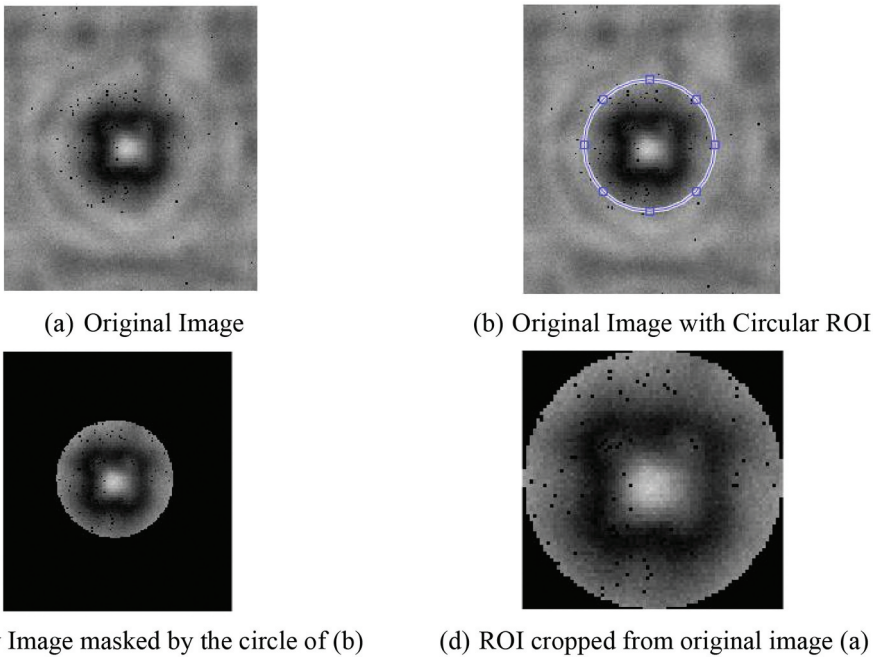

Figure 12. Solder joint post processed regions of interest (ROI). Four separate images of a solder joint illustrating the implementation of an adjustable elliptical mask used to further process the region of interest (ROI) after thresholding. Figure 12(a) shows the original image of a solder joint after thresholding. Figure 12(b) shows the original image Figure 12(a) with a circular ROI. Figure 12(c) shows the image obtained from the circle of Figure 12(b). Figure 12(d) shows the image of the ROI cropped from Figure 12(a) using the circle from Figure 12(c). Figure shows that an adjustable elliptical mask can be used to separate out the ROI of solder joints.

Table 3. Flip chip failure pattern.

0.8 mm ENIG flip chip no.	Cycles to failure 1 cycle = 4 minutes	Failure time in hours
U23	3	0.2
U26	14	0.933
U35	21	1.4
U39	23	1.533
U46	24	1.6
U34	29	1.933
U36	34	2.267
U27	45	3
U43	48	3.2
U20	53	3.533
U31	55	3.667
U40	57	3.8
U19	68	4.533
U28	86	5.733

4.4. Mean intensity and histogram analysis

This Section 4.4 presents a method developed for analysis of flip chip solder bond failures based on the signals acquired by AMI during lifetime tests. Table 3 shows the failure pattern of the flip chips of the 0.8 mm ENIG finish PCB.

Upon close observation of the failure Table 3, one can argue that the flip chips in the PCB can be classified into 3 categories based on their reliability performance. If we consider 86 cycles as the total expected lifetime of a flip chip, then flip chips with a lifetime of less than 25% of expected lifetime will be considered as the least reliable while those above 50% will be considered as the most reliable while those in between will have medium reliability. To visualise this classification, colour coding is introduced as explained below in Table 4 and illustrated in Figure 13. For flip chip labelling refer to Figure 1. As discussed, based on reliability criteria shown in Figure 13 three flip chips were selected for further image processing of ENIG finished PCBs: U19 (very reliable), U34 (medium reliability) and U26 (least reliable). The results pertaining to U19, U34 and U26 will be presented in detail, as representative of the range of characteristics found during the reliability tests.

After extracting the region of interest as illustrated in section 5.3, the mean intensity of all the solder joints in all the flip chips under consideration were calculated. Figure 14 shows a scatter plot for the mean intensity variation of all the solder joints of U19 at cycle 0, before the test, and at cycle 65, the last test cycle before complete failure. From the mean intensity calculation of the solder joints, it can be seen that as the vibration cycling progresses and flip chips start to fail, three types of solder joints can be identified.

To determine the characteristics of these three types of joints, histogram analysis of the solder joints was done at cycle 0 and at the last scan cycle data obtained just before complete failure for flip chips U19, U34 and U26. From the analysis, three joints have been selected to clearly define the characteristics of the three types of solder joints formed during cycling: joints 67, 84 and 108. Each flip chip and the relative position of the selected joints in the flip chip are shown in Figure 15. It should be noted the solder joint orientation for all the flip

Table 4. Colour coded reliability criteria.

Colour code	Criteria (X% cycles to failure)
Red: least reliable	$\chi \leq 25$
Yellow: medium reliability	$25 < X \leq 50$
Blue: most reliable	$X > 50$

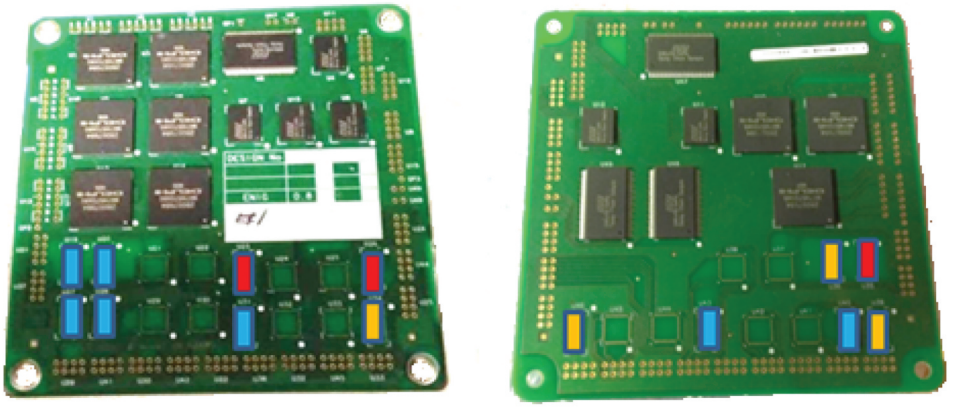

Figure 13. Generic board layout showing colour coded flip chip reliability (fully fractured joints) [19].

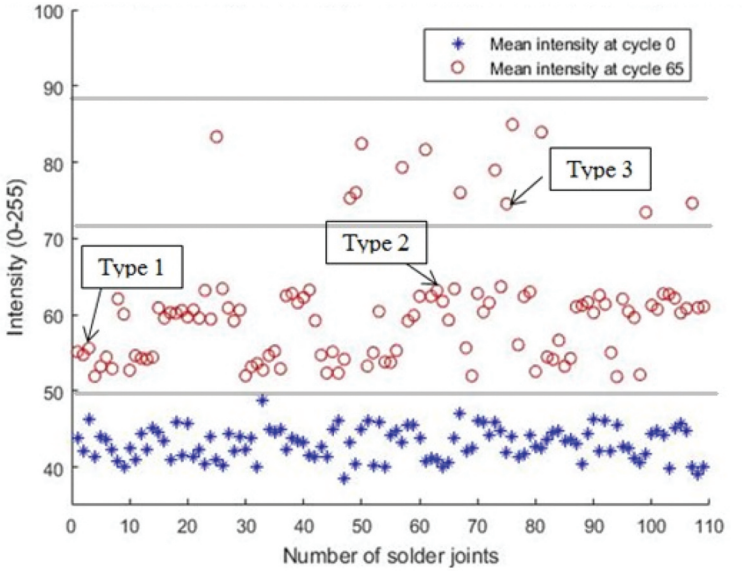

Figure 14. Mean intensity scatter plot for all the joints of U19.

chips is the same. The reason for selecting the joints 67 and 84, is that they are close to the centre of the flip chip, also known as neutral axis of the flip chip, and are also placed exactly opposite to each other. As a result, depending on the flip chip position, while one of them is near the edge of PCB the other is at the side away from the PCB edge. Hence analysing them not only showed the individual degradation pattern of the solder joints but also the degradation pattern with respect to the position of the flip chip in the PCB. Joint 108 was chosen because it is placed towards the corner of the flip chip and is also one of the only three joints placed furthest away from the chip edges, to help eliminate any possible 'edge' effects.

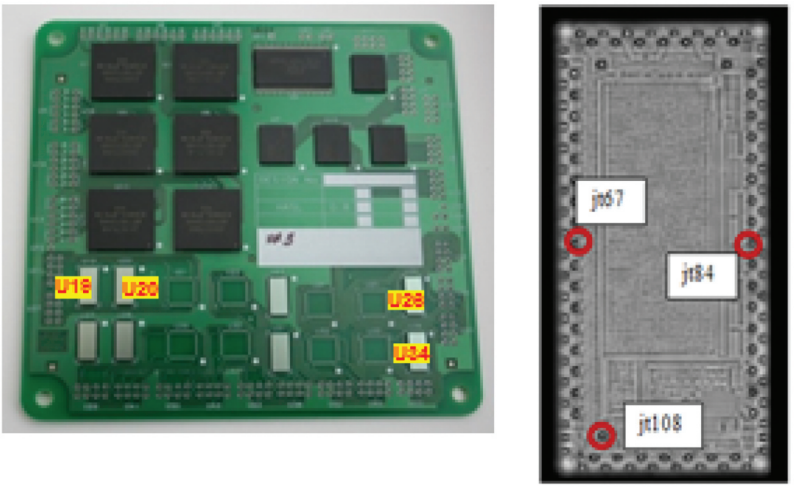

Figure 15. Selected flip chips and solder joints for further analysis.

Figures 16 –18show the results obtained from the histogram analysis of these three joints for each of the flip chips U19, U34 and U26. For chip U19, the centre frequency of joint 67 increases by 56% from 106 at 0 cycles to 165 at 65 cycles (Figure 16(a)), the centre frequency of joint 108 increases by 36% from 87.5 at 0 cycles to 118.75 at 65 cycles (Figure 16(b)), and the centre frequency of joint 84 increases by 15% from 100 at 0 cycles to 115 at 65 cycles (Figure 16(c)). For chip U34, the centre frequency of joint 67 increases by 16% from 106 at 0 cycles to 125 at 25 cycles (Figure 17(a)), the centre frequency of joint 108 increases by 32% from 106 at 0 cycles to 140 at 25 cycles (Figure 17(b)), and the centre frequency of joint 84 increases by 59% from 102 at 0 cycles to 162 at 25 cycles (Figure 17(c)). Finally, for chip U26, the centre frequency of joint 67 increases by 12% from 112 at 0 cycles to 125 at 12 cycles (Figure 18(a)), the centre frequency of joint 108 increases by 36% from 107 at 0 cycles to 145 at 12 cycles (Figure 18(b)), and the centre frequency of joint 84 increases by 65% from 76 at 0 cycles to 125 at 12 cycles (Figure 18(c)). Where the x axis represents pixel intensity, and the y axis represents the frequency of occurrence of each pixel intensity in each image. From the histogram analysis of the solder joints (three of which have been presented in detail above) as vibration cycling progresses, it can be concluded that there are three types of solder joints according to their increase in centre frequency near the time of complete failure of a flip chip. Based on the data collected and analysed for the remaining flip chips, the response was the same as shown in Figures 16–18, and may be summarised as:

(1) Type 1: Joints that show 9%–18% increase in intensity with cycling.
(2) Type 2: Joints that show 25%– 40% increase in intensity with cycling.
(3) Type 3: Joints that show 55%– 80% increase in intensity with cycling.

When the number of type 2 and type 3 joints exceed the number of type 1 joints, a flip chip fails. Based on research conducted by Yang [22], it was found that solder joints exhibiting a very low change in intensity during inspection at the end of Accelerated Thermal Cycle testing (ATC) relative to the intensity observed at the start of test or time zero were shown to be healthy joints. Conversely, those showing very high change of intensity at the end environmental testing were fractured joints. Similarly, it may be argued in the case of vibration, type 1 joints represent the healthy joints while type 3 will represent complete fracturing of a joint. Furthermore, Type 2 would be representative of partially fractured joints. Accordingly, Table 5 classifies joints 67, 84 and 108 of U19, U34 and U26 into types 1, 2 and 3 respectively.

Table 5 shows an interesting result that the position of the flip chip and solder joint's reliability varies with the position and orientation of the flip chip on a PCB. Solder joint 67 of U19 and joints 84 of U34 and U26 are all positioned nearest to the edge of the PCB and showed similar behaviour with lower reliability, compared to solder joint 84 of U19 and joints 67 of U34 and U26 that are all positioned on the flip chip side away from the edge of the PCB and exhibited higher reliability.

Now that the types of joints formed during vibration cycling have been classified, the next step was identification of how and when the crack forms and propagates in a particular solder joint. Mean intensity and area analysis of the solder joints gave suitable solutions.

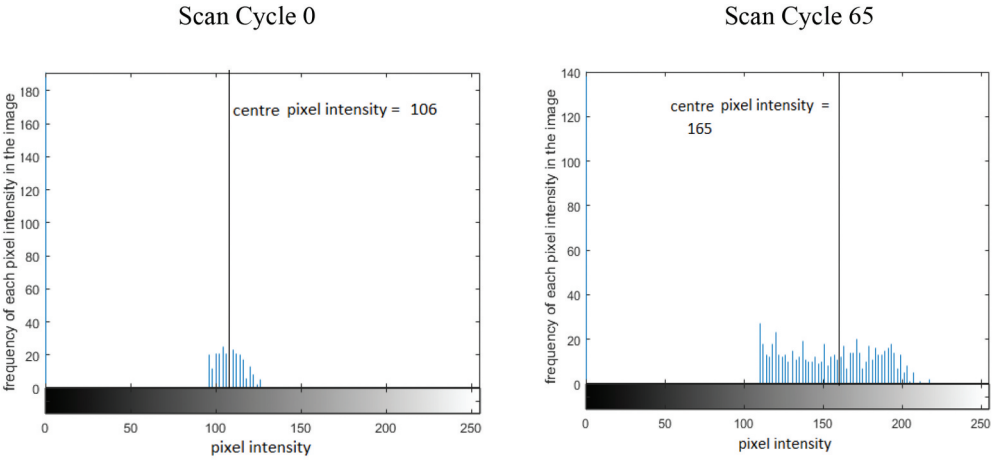

(a) Solder bump 67 of U19

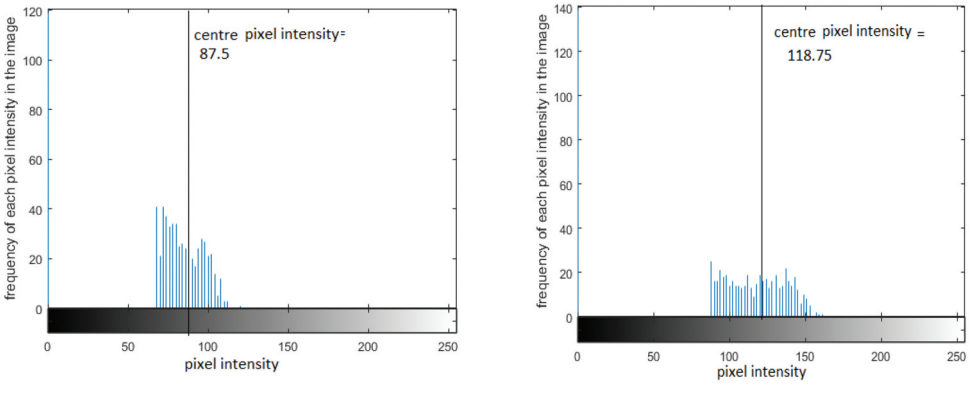

(b) Solder bump 108 of U19

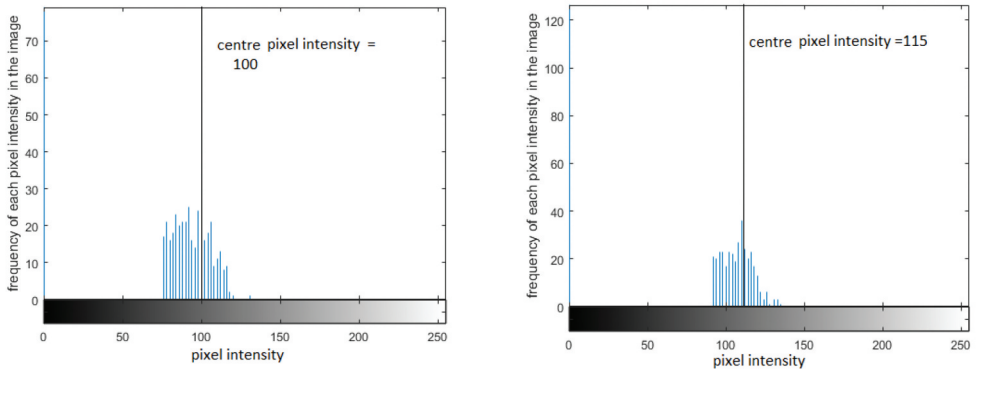

(c) Solder bump 84 of U19

Figure 16. Histogram analysis for U19 at cycle 0 and cycle 65 for (a) joint 67; (b) joint 108; (c) joint 84.

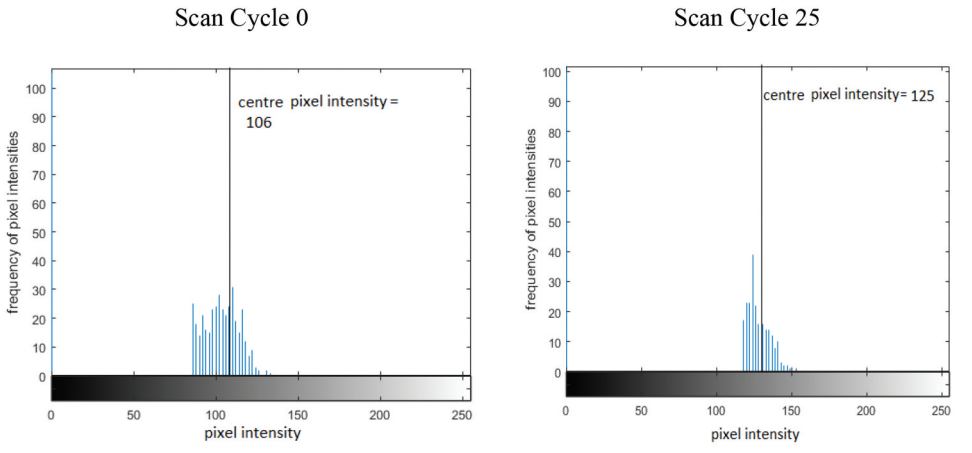

(a) Solder bump 67 of U34

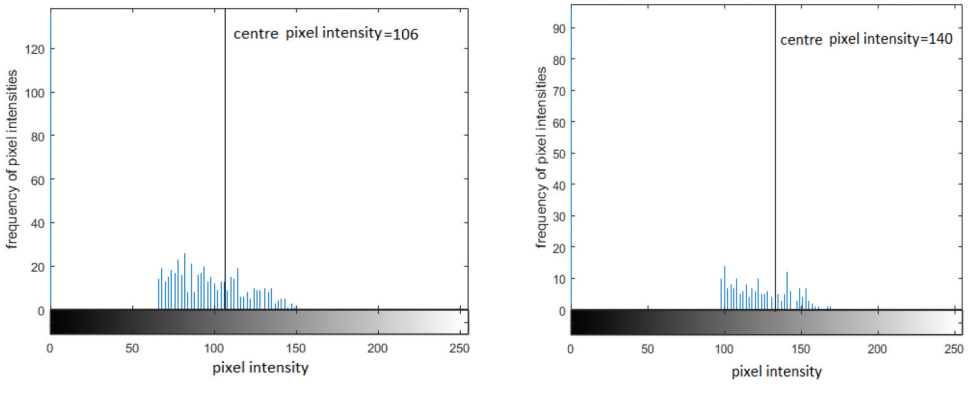

(b) Solder bump 108 of U34

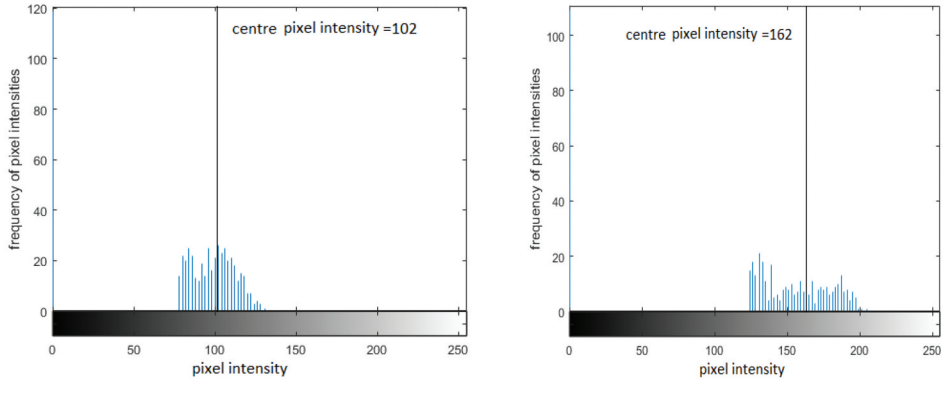

(c) Solder bump 84 of U34

Figure 17. Histogram analysis for U34 at cycle 0 and cycle 25 for (a) joint 67; (b) joint 108; (c) joint 84.

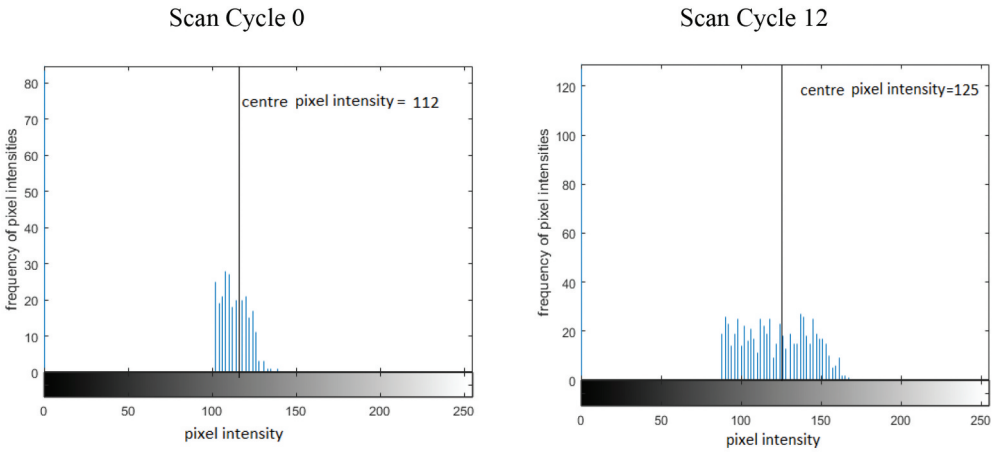

(a) Solder bump 67 of U26

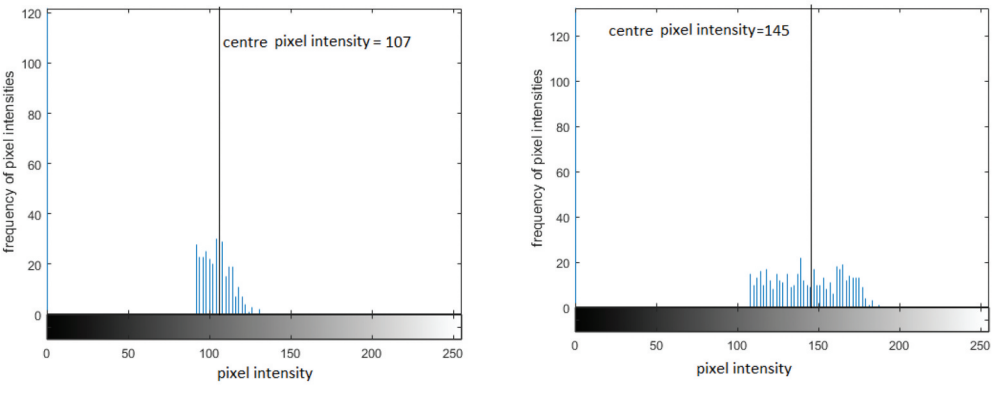

(b) Solder bump 108 of U26

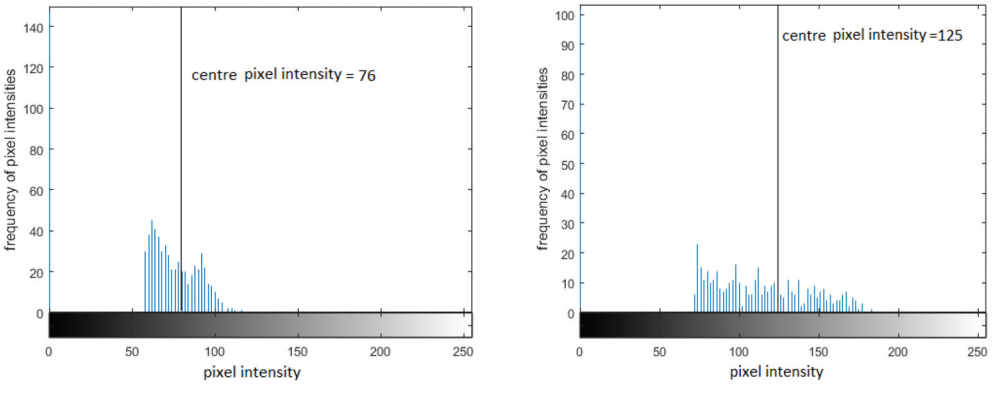

(c) Solder bump 84 of U26

Figure 18. Histogram analysis for U26 at cycle 0 and cycle 12 for (a) joint 67; (b) joint 108; (c) joint 84.

4.5. Mean intensity and area analysis

As in histogram analysis, the same flip chips U19, U34 and U26 and solder joints 67, 84 and 108 will be used to illustrate the results for mean intensity and area analysis.

Figures 19 and 20 illustrate the measured mean intensity values and area in pixels for the selected three solder of interest from time zero (T_0) representing zero cycles up to complete mechanical failure. From the mean intensity and area plots of U19 (Figure 19), it can be clearly seen that the first abrupt change in gradient of mean intensity/area, which will henceforth be referred to as the first trigger point occurs at 25 cycles (38.5% cycling),while the second abrupt gradient change which will be referred to as the second trigger point occurs at 55 cycles (84.5% cycling) for joints 67, 84 and 108. For flip chip U34 (Figure 20), the first trigger point occurs at 10 cycles (40% cycling), while the second trigger point occurs at 20 cycles (80% cycling). For U26 (Figure 21), the first trigger point occurs at 4 cycles (33.3% cycling), while the second trigger point occurs at 10 cycles (83.33% cycling).

The abrupt increase in the mean intensity and area of the ROI with the increase in the number of vibration cycles at the first and second trigger points of all the solder joints, clearly suggests the origin and propagation of cracks. However, depending on the type of solder joint as healthy, partially fractured or fractured, the resultant rise in mean intensity or area varies, which further validates the results obtained from the histogram analysis of the solder joints discussed in the previous section. For all types of joints in a flip chip, the first trigger point occurs at around 35–40% cycling and second change occurs at around 80–85% cycling. Thus, the failure pattern of any solder joint can be loosely said to fall into three regions. The region between 0 cycle and first trigger point where the crack initiates, the region between the first and second trigger point where the crack propagates and finally the region after the second trigger point where the crack formed reaches its peak which finally leads to flip chip mechanical failure.

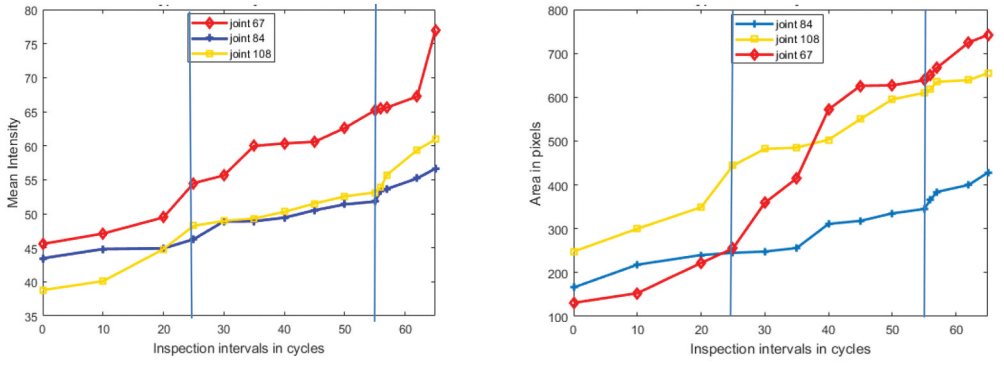

Figure 19. Variation of mean intensity (a) and area (b) for solder joints 67, 84 and 108 of U19. Two separate line graphs, each with three lines for solder joints 67, 84 and 108 of flip chip U19. Figure 19(a) displaying the mean intensity. Figure 19(b) displaying the area in pixels. The x-axis represents the number of inspection cycles ranging from 0 to 65. The graphs show a first abrupt change in gradient of mean intensity and area at 25 cycles, and a second abrupt gradient change at 55 cycles for the three joints.

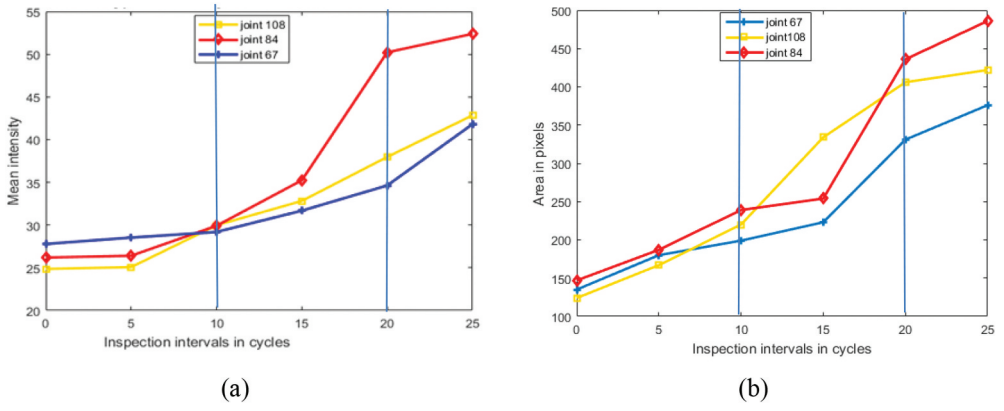

Figure 20. Variation of mean intensity (a) and area (b) for solder joints 67, 84 and 108 of U34. Two separate line graphs, each with three lines for solder joints 67, 84 and 108 of flip chip U34. Figure 20(a) displaying the mean intensity. Figure 20(b) displaying the area in pixels. The x-axis represents the number of inspection cycles ranging from 0 to 65. The graphs show a first abrupt change in gradient of mean intensity and area at 10 cycles, and a second abrupt gradient change at 20 cycles for the three joints.

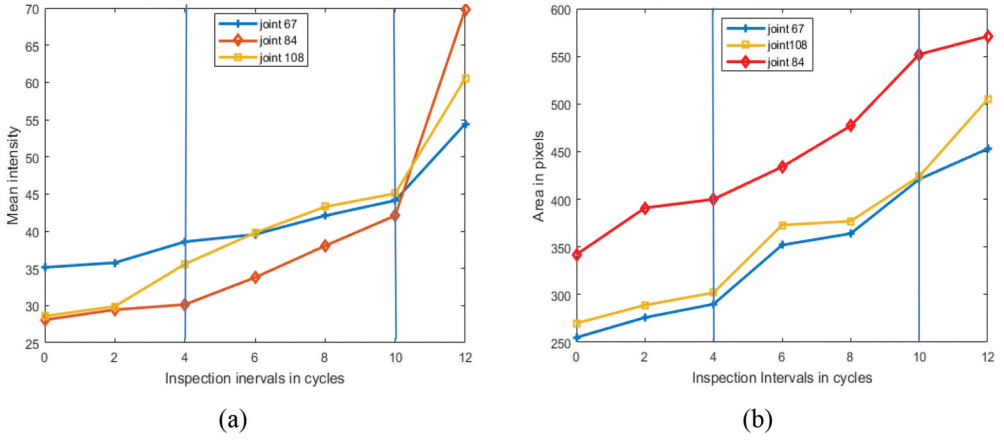

Figure 21. Variation of mean intensity (a) and area (b) for solder joints 67, 84 and 108 of U26. Two separate line graphs, each with three lines for solder joints 67, 84 and 108 of flip chip U26. Figure 21(a) displaying the mean intensity. Figure 21(b) displaying the area in pixels. The x-axis represents the number of inspection cycles ranging from 0 to 65. The graphs show a first abrupt change in gradient of mean intensity and area at 4 cycles, and a second abrupt gradient change at 10 cycles for the three joints.

Table 5. Classification of joints 67, 84 and 108 of chips U19, U34 and U26.

	Solder Joint Identifier		
Flip chip Identifier	Type 1 (Healthy)	Type 2 (Partial fracture)	Type 3 (Fractured)
U19	84	108	67
U34	67	108	84
U26	67	108	84

5. Weibull analysis

The Weibull distribution is one of the most common lifetime distributions utilised in reliability engineering to represent the reliability model for solder joints [25]. The time to failure from the vibration tests can be described using the equation for the Probability Density Function (PDF) of a Weibull distribution, f(t), which it is given by Reliability Engineering Resources [26]:

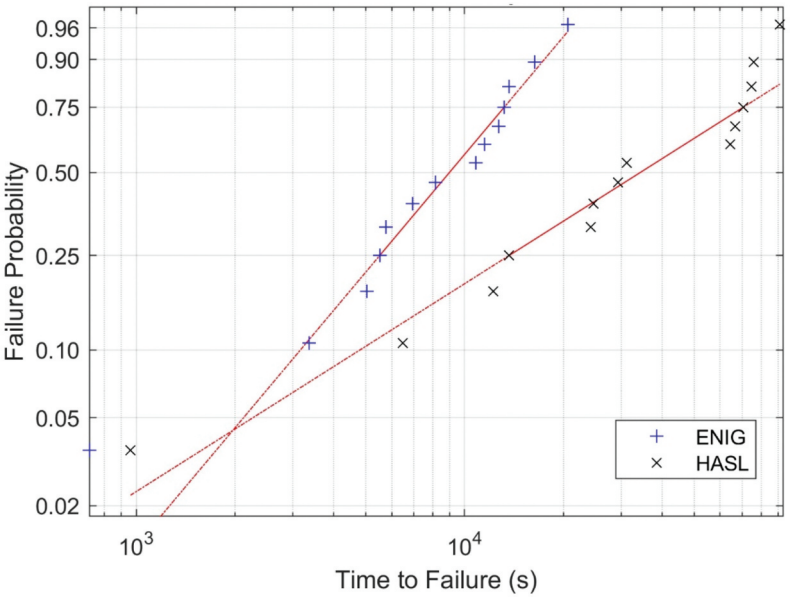

Figure 22. Weibull plots for Pb HASL and ENIG whole PCB/board vibration failures (Blue plus sign =ENIG, black cross symbol = Pb HASL) Weibull probability plot from vibration testing results, with two linear distributions for flip chips on Pb HASL finished PCBs (black cross markers) and ENIG finished PCBs (blue plus marker). The x-axis represents the time to failure in seconds in logarithmic scale. The y-axis represents the Weibull failure probability ranging from 0 to 1 in logarithmic scale. Pb HASL reliability reaches about 90,000 seconds, with a slope of 0.765. ENIG reliability reaches about 20,000 seconds, with a slope of 1.297.

Table 6. Flip chip cycle and failure times for ENIG and Pb HASL boards.

ENIG flip chip number	Cycles to failure 1 cycle = 4 minutes	Failure time in hours	Pb HASL flip chip number	Cycles to failure	Failure time in hours
U23	3	0.2	U23	4	0.267
U26	14	0.933	U26	27	1.8
U35	21	1.4	U27	51	3.4
U39	23	1.533	U34	57	3.8
U46	24	1.6	U19	101	6.733
U34	29	1.933	U28	103	6.867
U36	34	2.267	U20	122	8.133
U27	45	3	U46	130	8.667
U43	48	3.2	U36	268	17.867
U20	53	3.533	U39	278	18.533
U31	55	3.667	U35	294	19.6
U40	57	3.8	U31	311	20.733
U19	68	4.533	U43	316	21.067
U28	86	5.733	U40	380	25.333

$$f(t) = \frac{\beta}{\eta}\left(\frac{t-\gamma}{\eta}\right)^{\beta-1} e^{-}\left(\frac{t-\gamma}{\eta}\right)^{\beta} \quad (1)$$

where $f(t) \geq 0$ is the cumulative failure distribution function or failure rate, and $t \geq 0$ is the time to failure. The parameters β, η and γ control the shape, scale, and location of the probability density function. The shape parameter, $\beta > 0$, defines the shape of the distribution, the scale parameter, $\eta > 0$, defines where the bulk of the distribution lies, and the location parameter, $-\infty < \gamma < \infty$, defines the location of the distribution in time. The Weibull distribution can take on the characteristics of other types of distributions based on the value of its shape parameter β, which is equal to the slope of the regressed line in a probability plot. The value of β has a marked effect on the failure rate of the Weibull distribution. Inferences can be drawn about a population's failure characteristics just by considering whether the value of β is less than, equal to, or greater than one. Populations with $\beta < 1$ exhibit a failure rate that decreases with time, populations with $\beta = 1$ have a constant failure rate that is consistent with an exponential distribution, and populations with $\beta > 1$ have a failure rate that increases with time. Figure 22 shows the Weibull probability plots of Table 6.

The two Weibull plots in Figure 22 show the different reliability characteristics for ENIG and Pb HASL finished PCBs found from vibration testing. A clear difference in the lifetime characteristics can be seen for the two surface finishes on the PCBs. The long-term reliability of Pb HASL is best typically extending to over 380 × 4 minutes/cycle or about 90,000 seconds, compared to ENIG that only reaches about 90 × 4 minute cycles or about 20,000 seconds. The shape parameter β [25] has been calculated to be $\beta = 0.765$ for Pb HASL, which being less than 1 indicates that the materials set accumulates more failures initially, with an increase in failure rate at a lower number of cycles. The lower slope of the Pb HASL plot however, indicates a longer overall lifetime. The shape parameter $\beta = 1.297$ being greater than 1, indicating that the ENIG material set has a more consistent behaviour with a more constant failure rate. The higher slope of the ENIG plot indicates a reduced overall lifetime. Thus, these results show that the PCB's surface finish strongly affects the lifetime of the solder joints, and with the use of Pb HASL some solder joints failed with the shortest lifetimes but exhibited better overall vibration resistance.

6. Results and discussion

From the analysis of the ultrasound or acoustic images obtained from AMI it has been found that:

(i) The grey region in the middle of the solder joints varied according to the quality of the connection between silicon die and solder joint. The intensity and area of this region for a partially fractured or fractured joint tends to be higher compared to a healthy joint.
(ii) Three types of solder joints have been found to be formed near the time of complete failure of a flip chip:

Type 1 or healthy: Joints that show 9%–18% increase in intensity with cycling
Type 2 or partially fractured: Joints that show 25%– 40% increase in intensity with cycling

Type 3 or fractured: Joints that show 55%– 80% increase in intensity with cycling

(iii) Two trigger points in the lifetime of any solder joint have been identified from the mean intensity and area analysis. The first trigger point suggests crack initiation and occurs at around 35%-40% cycling, and the second trigger point which refers to the path of crack propagation occurs at around 80%–85% cycling. However, depending on whether the joint is healthy, partially fractured or fractured, the resultant rise in mean intensity or area varies. Hence, the failure pattern of any solder joint can be classified to fall under three regions. The region between zero cycle and first trigger point where the crack initiates, the region between the first and second trigger point where the crack propagates, and finally the region after the second trigger point where the crack formed reaches its peak and the flip chip joint fails.
(iv) When about 70%–80% of the solder joints in a flip chip are either partially fractured or fractured the flip chip was found to fail in the next few vibration cycles.

7. Conclusions

In this paper, the effects of vibration reliability testing representing spectral energy observed in automotive environments on the reliability of solder joints in an industry grade PCB were analysed. Non-destructive testing in the form of acoustic micro imaging was used for through-life data collection and MATLAB was used for data analysis. This study was able to estimate two trigger points within the lifetime of a solder joint, the first of which detected crack initiation at around 35–40% of their lifetime, while the second trigger point indicated the point just before complete mechanical failure, tracked at around 80–85% of a solder joints lifetime.

Knowledge of these trigger points will save a lot of time and resources in an industrial vibration environment where otherwise devices are tested until complete failure and can take several months for testing. However, now that the first trigger point of probable crack initiation can be found, devices can be tested and monitored until this point and if signs of crack initiation do appear the prognostics of future health can be used to predict solder joint lifetime without completing a full test to failure, resulting in a much more efficient use of time and resources.

Acknowledgements

This research was partially supported by the British Council Newton-Ungku Omar Fund Institutional Links [Green Electronics Project ID: 332397914], and the EU H2020-MSCA-RISE -2019 [Reactive Too Project: 871163].

Disclosure statement

No potential conflict of interest was reported by the author(s).

Funding

The work was supported by the EU H2020-MSCA-RISE-2019 [871163]; British Council Newton-Ungku Omar Fund Institutional Links [332397914].

References

[1] Meier K, Leslie D, Dasgupta A, et al. Analysis of flip-chip solder joints under isothermal vibration loading. In: IEEE 21st Electronics Packaging Technology Conference (EPTC); 2019, p. 138–142.
[2] Eckert T, Muller WH, Nissen NF, et al. A solder joint fatigue life model for combined vibration and temperature environments. In: 59th Electronic Components and Technology Conference (ECTC); 2009, p. 522–528.
[3] Vaion RE, Medda M, Mancaleoni A, et al. Qualification extension of automotive smart power and digital ICs to harsh aerospace mission profiles: gaps and opportunities. Microelectron Reliab. 2017;76-77(77):438–443.
[4] Johnson RW, Evans JL, Jacobsen P, et al. The changing automotive environment: high-temperature electronics. IEEE Trans Electron Packag Manuf. 2004;27(3):164–176.
[5] Jiang N, Zhang L, Liu Z-Q, et al. Reliability issues of lead-free solder joints in electronic devices. Sci Technol Adv Mater. 2019;20(1):876–901.
[6] Aircraft accident investigation report KNKT.14.12.29.04 PT. Indonesia Air Asia, Airbus A320-216; PK-AXC, Karimata Strait, Coordinate 3°37'19"S - 109°42'41"E, KOMITE NASIONAL KESELAMATAN TRANSPORTASI, Republic of Indonesia, 28 December 2014 Republic of Indonesia; 2015.
[7] Steinberg DS. Vibration analysis for electronic equipment. 3rd ed. Wiley: New York; 2000. ISBN:978-0-471-37685-9
[8] Tummala RR, Rymaszewski EJ, Klopfenstein AG. 1997. Microelectronics packaging handbook. 2nd ed. New York: Chapman and Hall.
[9] Choi K, Yu D-Y, Ahn S, et al. Joint reliability of various Pb-free solders under harsh vibration conditions for automotive electronics. Microelectron Reliabil. 2018;86:66–71.
[10] An T, Fang C, Qin F, et al. Failure study of Sn37Pb PBGA solder joints using temperature cycling, random vibration and combined temperature cycling and random vibration tests. Microelectron Reliabil. 2018;91:213–226.
[11] Kim YK, Hwang DS. PBGA packaging reliability assessments under random vibrations for space applications. Microelectron Reliab. 2015;55(1):172–179.
[12] Yu D, Al-Yafawi A, Nguyen TT, et al. High-Cycle fatigue life prediction for Pb-free BGA under random vibration loading. Microelectron Reliab. 2011;51(3):649–656.
[13] Muhammad N, Fang Z, Shoaib M. Remaining useful life (RUL) estimation of electronic solder joints in rugged environment under random vibration. Microelectron Reliab. 2020;107:113614.
[14] Lall P, Lowe R, Goebel K. Prognostication of accrued damage in board assemblies under thermal and mechanical stresses. In: IEEE 2012 IEEE 62nd Electronic Components and Technology Conference; 2012, p.1475–1487.
[15] Che FX, Pang JHL. Study on reliability of PQFP assembly with lead free solder joints under random vibration test. Microelectron Reliab. 2015;55(12):2769–2776.
[16] Braden DR, Yang RSH, Duralek J, et al. Investigation into the impact of component floor plan layout on the overall reliability of electronics systems in harsh environments. In: 3rd Electronics System Integration Technology Conference ESTC; 2010, pp. 1–6.
[17] Yang RSH, Braden DR, Zhang G-M, et al. An automated ultrasonic inspection approach for flip chip solder joint assessment. Microelectron Reliab. 2012;52(12):2995–3001.
[18] Nordson/Sonoscan. Nordson Test and Inspection: Acoustic Products; 2021 [cited 2021 Jun 1]. Available from: https://www.nordson.com/en/divisions/sonoscan/support/faqs.

[19] Baishya K. Through-life monitoring of the impact of vibration on the reliability of area array packages using non-destructive testing [PhD Thesis]. LJMU, UK; 2019. oai:researchonline.ljmu.ac.uk:10654
[20] Baishya K, Harvey DM, Zhang G, et al. Investigation into how the floor plan layout of a manufactured PCB influences flip-chip susceptibility to vibration. IEEE Trans Compon Packag Manuf Technol (CPMT). 2020;10(5):741–748.
[21] Yang SH. Through-life non-destructive monitoring of solder joints using ultrasound [PhD Thesis]. GERI, LJMU: Liverpool, UK; 2012.
[22] Otsu N. A threshold selection method from gray-level histograms. IEEE Trans Syst Man Cybern. 1979;9(1):62–66.
[23] Glasbey C. An analysis of histogram-based thresholding algorithms. CVGIP Graphical Models Image Process 55; 1993, 532–537.
[24] Henstock PV, Chelberg DM. Automatic gradient threshold determination for edge detection using a statistical model a description of the model and comparison of algorithms. ECE Technical Report TR-ECE 96-13; 1996. [cited 2021 June 1]. Available form: http://docs.lib.purdue.edu/ecetr
[25] Elsayed EA. Reliability engineering. 2 ed. Hoboken, New Jersey, USA: Wiley; 2012. ISBN:1-118-30950-2.
[26] Reliability engineering resources. 2001 [cited 2021 Jun 1]. Available from: https://www.Weibull.com